JOURNAL OF PROPULSION AND POWER
Vol. 28, No. 6, November–December 2012

Simple Analysis of Flame Dynamics via Flexible Convected Disturbance Models

Joseph A. Ranalli* and Donald Ferguson†
National Energy Technology Lab, Morgantown, West Virginia 26507
and
Christopher Martin‡
Virginia Polytechnic and State University, Blacksburg, Virginia 24060

DOI: 10.2514/1.B34405

Flame sheet modeling is a common approach for the determination of flame transfer functions for prediction and modeling of thermoacoustic combustion instabilities. The dynamics of the flame-sheet model for simple flame geometries can be shown to be equivalent to a basic model of convective disturbances interacting with a steady heat release region. This framework shows that the flame transfer functions predicted by linearized flame-sheet models are the Fourier transform of the steady heat release rate profile for the flamesheet geometry transformed into a Lagrangian convective time reference frame. This result is significant relative to existing flame-sheet modeling approaches in allowing the prediction of dynamic behaviors on the basis of steady information only. Multiple perturbations on the flame can be treated simply via superposition of individual perturbations. Analysis of results from these convective disturbance models illuminates the existence of two independent length scales governing the flame transfer function dynamics. Magnitude is governed by the tip-to-tail length of the flame, whereas phase is governed by the heat release rate profile center of mass calculated from the disturbance origin. The convective disturbance approach shows promise in its potential to derive flame transfer function predictions from a steady flame heat release rate profile.

Nomenclature

d	=	convective liftoff from shedding location, s
f	=	frequency, Hz
K	=	ratio of flow to convection velocity
L_f	=	tip-to-tail axial length of the flame, m
Q	=	global flame heat release rate, W
q	=	localized flame heat release rate, W/s
R	=	radius of flame, m
r	=	radial distance, m
St	=	Strouhal number
S_u	=	turbulent flame speed, m/s
t	=	time, s
u	=	axial velocity, m/s flame-sheet
$V(\lambda)$	=	distribution characteristic function
x	=	axial distance, m flame-sheet
x_{com}	=	axial intensity weighted flame center of mass, m
x_0	=	steady component of x
x_1	=	oscillating component of x
α	=	ratio of flame length to flame radius
β	=	$\alpha^2(\alpha^2+1)^{-1}$
θ	=	angle from dump plane to steady flame-sheet, rad
λ	=	convective Strouhal number
$\xi(r,t)$	=	axial distance to flame-sheet surface, m/s
τ	=	convective time delay, s
Φ	=	equivalence ratio
ψ	=	convective heat release rate profile, W/s
ω	=	angular frequency, rad/s

Received 25 July 2011; revision received 20 January 2012; accepted for publication 28 January 2012.

*Postdoctoral Research Assistant; currently Assistant Professor of Engineering at Penn State University Hazleton; jar339@psu.edu. Member AIAA.
†Research Engineer; donald.ferguson@netl.doe.gov. Member AIAA.
‡Research Associate; chmarti1@vt.edu.

I. Introduction

THERMOACOUSTIC instabilities pose a significant problem to the reliability and operability of gas turbine combustor performance. This phenomenon is characterized by oscillations in the flame heat release rate that become coupled with the system acoustics, resulting in disturbances that present a potential physical hazard to hardware [1]. In order to mitigate this problem, research efforts have been aimed at increased understanding of the nature of these instabilities. A complete description of the flame behavior, both through analytical modeling and experimental validation, can provide the necessary framework for this problem to be understood and subsequently eliminated in practical systems. While state-of-the-art modeling approaches have proved successful at predicting the flame transfer function for specific cases, further work is needed to extend these modeling approaches to include a wider variety of flame geometries.

Periodic disturbances in the velocity field and/or fuel–air mixing are considered the primary coupling mechanisms between oscillations in the flame heat release and system acoustics. This coupling process may be described by a block diagram such as that shown in Fig. 1. Oscillations in pressure (p') have previously been shown not to play a significant role in the flame dynamics [2], though both velocity and equivalence ratio oscillations are known to lead to instabilities.

The type of closed-loop model shown in Fig. 1 suggests use of a "black-box," transfer function–based analysis of the system dynamics. While the dynamics of the acoustics and mixing process, although nontrivial, may be obtained through models or experiments, a complete understanding of the flame dynamics still presents a significant research challenge. As novel combustor designs and a wider variety of fuel stocks are used in the future, this problem may be exacerbated, and continued research is needed to ensure continuity of safe, reliable operation.

II. Background

A. Analysis of Flame Transfer Functions in Literature

Theoretical and experimental consideration has been given to determining the flame transfer function (FTF) for flames of both

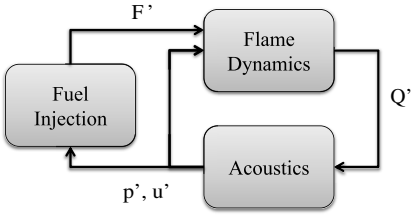

Fig. 1 Closed-loop model describing the coupling leading to thermoacoustic instabilities.

conical and inverted-conical (V-flame) shapes, in both laminar and turbulent flow regimes [3–13]. Typically, the FTF is described as the flame (or more specifically the heat release) response to velocity perturbations and is commonly written in a form normalized by the mean values:

$$\mathrm{FTF} = \frac{Q'/\bar{Q}}{u'/\bar{u}} \tag{1}$$

Recent theoretical studies have focused on the use of flame-sheet models, which consider the flame to be a thin sheet that responds to perturbations in the flow. In essence, flame-sheet modeling is a kinematic approach, in which the time-resolved position of the flame surface is determined by the competing forces of the surface being convected along with the flow and propagation of the flame into the unreacted gases. This model approach provides the capability of predicting the flame location for a given flow field, but is practically limited in its capacity to analytically solve only relatively simple flow fields. Practical laboratory turbulent flames may exhibit additional behaviors, such as wall interactions with the enclosure, that have not yet been adequately produced within the flame-sheet framework. As will be shown, flame-sheet model results are strongly dependent on the exact shape of the heat release rate distribution, so the ability to precisely reproduce experimental distributions may be somewhat limiting.

Flame-sheet models have been extensively applied to prediction of laminar flame dynamics [3,14–17]. More recently, they have been extended to turbulent flames [18,19] by decomposition of the flame response into steady, stochastic (turbulent) and coherent (i.e., acoustic) perturbations. Another characteristic of recent flame-sheet modeling studies is consideration of the occurrence of explicit convective perturbations (e.g., convected vortices shed in-phase with the acoustics) instead of simple bulk acoustic oscillations [20,21]. Many of these models have been favorably validated with respect to experimental flame dynamics data [19].

One basis of flame-sheet model validation efforts is the FTF, with the following primary characteristics of the FTF found commonly in this literature:

1) Low-pass filter behavior, that is, a response occurs at low frequencies of excitation and dies off as the frequency increases.

2) The flame transfer function behavior can be nondimensionalized in frequency ω by the Strouhal number, using characteristic length x_c and convective velocity u_c scales indicating the importance of convective phenomena.

$$St = \frac{\omega x_c}{u_c} \tag{2}$$

3) Flame transfer function phase is dominated by convective delay.

4) Interference effects influence the response, attributed to different sources in the literature. Either localized, out-of-phase disturbances that interfere when computing the global response [4], or interference due to multiple perturbations acting simultaneously [22].

B. Characteristic Length and Velocity Scales

One shortcoming in both the experimental and theoretical flame dynamics literature is the lack of a unified methodology for nondimensionalization of the flame transfer function. While the concept of characteristic length and velocity scales is well understood, significant variation of opinion exists among investigators as to the source of these characteristic scales considered. Further, ambiguities in terminology are common, along with a lack of detail about calculation methods used, making direct reproduction or comparison of results difficult. The following literature review uses the referenced authors' own terminology and provides as much detail as provided in their original works, in order to highlight this difficulty.

Lohrmann and Büchner [5] used the "axial position of the main reaction region" with the axial volumetric convective velocity. In apparent contrast, Kim and Park [6] used distance to the "center of mass" accounting for both radial and axial displacement, obtained from Abel deconvoluted chemiluminescence images, and used velocity scaling from the transfer function phase delay. This assumes the disturbance propagates faithfully along the flame surface and not in a true bulk stream fashion. Kim et al. [23] appear to use the same scaling, but adopt terminology of the "distance to the maximum chemiluminescence intensity point." Palies et al. [19] used the injection tube diameter and the bulk injector tube velocity. Like Lohrmann and Büchner [5], Ranalli [24] used the straight axial distance to intensity weighted center of mass and the mean injector tube velocity. As stated, the lack of detailed descriptions of the scaling parameters used in these studies limits readers to what can be inferred from their terminology. In theoretical (i.e., flame-sheet) modeling studies, it is common to see nondimensionalization by either A) the flame length and the "convective velocity" often times related to the bulk volumetric velocity [21], or B) the duct radius and parameters related to the flame angle and flame speed [3,18,20]. Due to the interdependence between flame angle, flame length, flame speed, and flow velocity in a flame-sheet model, these may actually result in similar or identical nondimensionalizations.

As stated, the wide disparity in nondimensional length and velocity scales (or in ratio: convective time scales) used experimentally by different researchers makes unification of results between studies difficult. Nondimensionalizations that succeed in one particular study may depend heavily on geometry or may be somewhat fortuitous due to proportionality of parameters (e.g., for anchored flames, length is approximately proportional to center of mass offset [5,7]). Proportionality of parameters results in similar scaling of the dynamics but causes an inability to differentiate the physical behaviors of the individual parameters independently. Because of the lack of detail in describing the methods used to determine characteristic length scales from flame images, repetition of results is difficult and the lack of a unified methodology is further confounded. Comparisons between experimental and theoretical studies introduce additional difficulty because of the reliance on hard-to-quantify parameters (such as the turbulent flame speed) in flame-sheet model literature, over geometric parameters that can be easily related to experimental quantities.

As consideration is made of generalizing flame dynamic behaviors, these issues will become more significant. For example, the physical bases found within literature do not provide a solid framework in which to consider lifted flame geometries (such as with a low-swirl injector [24,25]) that have an uncertain characteristic length but exhibit similar dynamic behaviors to more traditional flame geometries [8]. Questions arise about whether liftoff distances should be included in characteristic length (i.e., measurement of length from the dump plane) or whether measurements should begin at the leading edge of the flame surface. This study aims to provide a model framework whose physics resemble those observed in experiments but relies on parameters in close conjunction with experimental data for developing further understanding of flame transfer functions with an emphasis on understanding of the governing physics.

III. Modeling Approach

The model detailed herein is based on a field of convected disturbances that interact with the flame in a spatially resolved manner. Results reflect the occurrence of both spatial and temporal interference, which lead to significant behaviors in the predicted flame transfer function and can be easily compared with

experimental data. This framework can be shown to be related to existing linearized flame-sheet models and can reproduce existing results for traditional flame geometries but allows for greater ease in variation of characteristic parameters and flame geometry.

A. Flame-Sheet Model Solution

The following is a brief summary of linear flame-sheet modeling. For further details of the derivation and origin of these models, readers are encouraged to consult more comprehensive sources in literature [18,20,21]. Flame-sheet model results are obtained though calculation of the flame surface position ξ as a function of time and space by solution of the following equation:

$$\frac{\partial \xi}{\partial t} = u - S_u \sqrt{\left(\frac{\partial \xi}{\partial r}\right)^2 + 1} \tag{3}$$

This form of the equation relies on the assumption of a purely axial velocity. The basic physics described by this equation state that the motion of the flame surface is the net result of the balance between convection of the surface by the flow and the flame propagation into the unburned region. As the second term on the right-hand side is nonlinear, the solution requires linearization that can be performed through Taylor Series expansion about the mean flame position ξ_0. As stated, recent flame-sheet model studies have considered the flame response to velocity perturbations described by an explicitly convective (e.g., vortical) perturbation as follows:

$$u_1(r,t) = a_u e^{j\omega(t - K\frac{\xi_0}{u_0})} \tag{4}$$

The parameter K is the ratio of the mean flow velocity to the velocity at which disturbances are convected by the flow (see [21]).

For a V-flame, stabilized on a centerbody at radius $r = 0$, the linearized solution for Eq. (3) subject to this excitation can be shown as follows:

$$\xi_1 = \frac{a_u}{j\omega} \frac{e^{j\omega(t - \frac{1}{S_u\sqrt{\beta}}r)} - e^{j\omega(t - \frac{\alpha K}{u_0}r)}}{\beta K - 1} \tag{5}$$

We have defined two parameters to simplify the presentation:

$$\alpha \equiv \frac{\partial \xi_0}{\partial r} = \frac{L_f}{R} \quad \text{and} \quad \beta \equiv \frac{\alpha^2}{\alpha^2 + 1}$$

Note that by this terminology, $\alpha = \tan\theta$ and $\beta = \sin^2\theta$ where θ is the angle between the dump plane and the steady flame surface. The oscillating surface response in Eq. (5) is the combined result of the convective disturbance and a second, similar response that travels along the flame surface, arising due to the flame anchoring [21].

The global heat release rate for the flame-sheet model is calculated by integrating Eq. (5) based on the desired flame geometry to reach the total flame surface area. By calculating the dynamic heat release rate response in this way, dividing by the oscillating velocity (i.e., at the dump plane) and normalizing by the means, we can obtain the flame transfer function [see Eq. (1)]. The form of integration for the global heat release rate depends on the flame geometry being considered, but as will be shown, a somewhat general final form can be reached. Consider the flame transfer function result for a V-flame in an axisymmetric geometry:

$$\mathrm{FTF}_a = \frac{2\beta^2}{St^2} \frac{1}{K(\beta K - 1)} \left\{ K\left[1 - e^{-j\frac{St}{\beta}}\left(1 + j\frac{St}{\beta}\right)\right] - \frac{1}{\beta}[1 - e^{-jStK}(1 + jStK)] \right\} \tag{6}$$

The Strouhal number used here is based on the axial length of the flame measured from the attachment point and the mean flow velocity, similarly to Preetham et al. [21].

$$St \equiv \frac{\omega L_f}{u_0}$$

By substituting for differences in terminology and manipulating, Eq. (6) can be shown to be equivalent to the results given in literature [20,21]. This equation is described in literature as reflecting the response of two perturbations: a flame front disturbance (flame "wrinkle") associated with interactions at the attachment point and the affect of the explicit convective perturbation described in the nonuniform velocity disturbance, Eq. (4). One interesting characteristic not described in literature is that the responses in Eq. (6) for each of the two perturbations actually have identical forms. This can be highlighted by considering the limit of Eq. (6) as the convective disturbance is neglected ($K \to 0$).

$$\lim_{k\to 0} \mathrm{FTF}_a = -\frac{2\beta^2}{St^2}\left[1 - e^{-j(St/\beta)}\left(1 + j\frac{St}{\beta}\right)\right] \tag{7}$$

This result bears a similar form to the individual terms in Eq. (6). If we consider Eq. (7) to be a function of an arbitrary parameter λ, we can find the following characteristic function for the dynamics of an axisymmetric V-flame.

$$V_a(\lambda) = -\frac{2}{\lambda^2}[1 - e^{-j\lambda}(1 + j\lambda)] \tag{8}$$

Substituting Eq. (8) into Eq. (6) then yields the following general equation for the flame-sheet flame transfer function.

$$\mathrm{FTF} = \frac{1}{1 - \beta K}\left[V\left(\frac{St}{\beta}\right) - \beta K V(KSt)\right] \tag{9}$$

In fact, this same result can be achieved for other geometries in which the system obeys the flame-sheet surface behavior described in Eq. (5). Computing the flame transfer function of a bluff-body stabilized V-flame results in the exact same form for Eq. (9), albeit with a different form for the geometry dependent characteristic function $V(\lambda)$.

$$V_{BB}(\lambda) = \frac{1}{j\lambda}(1 - e^{-j\lambda}) \tag{10}$$

Thus, the flame-sheet model flame transfer function solution can be seen to be the linear combination of two individual disturbances, a flame wrinkle convected along the flame surface and a bulk flow convective perturbation as described above. Significantly, these disturbances each interact with the flame in exactly the same way, although each moves at a different convective speed. Variability in linear flame transfer functions described in literature primarily reflect differences in the characteristic function $V(\lambda)$, brought about only by changes in the flame geometry considered, but maintain a general combined form [Eq. (9)]. Thus, study of the response leading to the characteristic function on a single perturbation basis could lead to a better understanding of the physics of the compounded disturbance.

B. The Convected Disturbance Model

A different one-dimensional (1-D) modeling approach, termed a convected disturbance model, will be derived and shown to be capable of reproducing the linearized flame-sheet modeling results described in the previous section. Note that this model is different than flame-sheet models in that it does not attempt to predict the flame structure, but rather depends on a known flame heat release rate distribution as an input (i.e., steady state flame heat release profile). The convected disturbance model used in this study is based on the following thought experiment:

1) Consider a 1-D flow field, drawn from left-to-right in Fig. 2. The spatially dependent variable τ is written in terms of convective time as measured travelling at some arbitrary convective velocity u_c from a given origin (x_0).

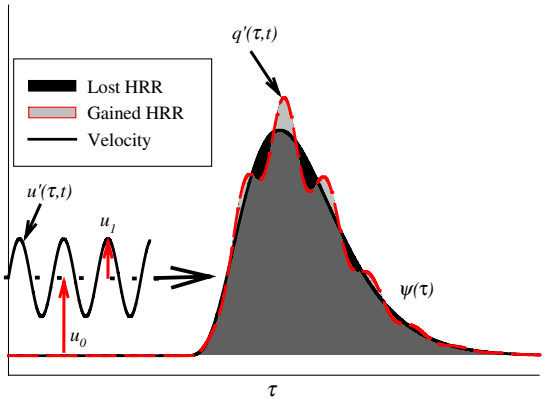

Fig. 2 Sketch of convective disturbance model behavior.

$$\tau(x) \int_{x_0}^{x} \frac{\mathrm{d}\dot{x}}{u_c(\dot{x})} \xrightarrow{\text{for constant } u_c} K\frac{x}{u_0} \tag{11}$$

2) An arbitrary, 1-D steady region of heat release in space represents local flame heat release rate.

3) Perturbations in the mass flow rate u_1 arise from an arbitrary location in the flow field and are convected with the bulk flow through the heat release region.

4) As they reach the flame, the velocity disturbances induce local heat release rate perturbations q_1, which are directly proportional to the amplitude of the local velocity disturbance and the local intensity of the axial heat release rate profile ψ. Mathematically,

$$q_1(\tau, t) = u_1(\tau, t)\psi(\tau) \tag{12}$$

5) Eq. (11) can then be integrated over all τ to yield the global flame heat release rate $Q'(t)$.

A sketch of this overall behavior is shown in Fig. 2. As stated, the unsteady global heat release rate is then the integral over all convective time of the heat release disturbances caused by this oscillating velocity. Due to the convective transformation, this is equivalent to the convolution of the convective oscillating velocity with the heat release rate profile also in convective space:

$$Q_1(t) = \int_0^{\infty} u_1(t-\tau)\psi(\tau)\,\mathrm{d}\tau = u_1 * \psi \tag{13}$$

where $\psi(\tau)$ is the steady heat release rate profile defined in a convective time reference frame (i.e., the time history of heat release rate experienced by a particle moving with the convective flow). This form results in the convenient result that the frequency domain flame transfer function is independent of the velocity disturbance. The transfer function then depends only on the Fourier transform of the convective steady heat release profile:

$$\mathrm{FTF} = \mathcal{F}\left(\frac{Q_1/Q_0}{u_1/u_0}\right) = \frac{\mathcal{U}_1(j\omega)\Psi(j\omega)/Q_0}{\mathcal{U}_1(j\omega)/u_0} = \frac{\Psi(j\omega)}{Q_0/u_0} \tag{14}$$

Recall that this result represents the global response of the flame to a single perturbation in the velocity. Due to the linearity of the Fourier transform, the response to multiple perturbations simply requires linear combination of multiple responses (or linear combination of the heat release profiles). As an example, consider the heat release profile (i.e., the flame surface area per unit axial distance) of an axisymmetric V-flame with disturbances arising at the flame anchoring point. This corresponds to a linear heat release rate distribution, due to the linearly increasing radius of the conical geometry:

$$\psi_a(\tau) = \tau\left[H(\tau-0) - H\left(\tau - \frac{\lambda}{\omega}\right)\right] \tag{15}$$

where $H(\tau-0)$ is the unit-step (Heaviside) function. The Fourier transform of this profile normalized to its mean is identically Eq. (8). This indicates that the physics described by this model are the same physics as modeled by a flame-sheet model responding to a single flow disturbance. Applying a linear combination of the characteristic function at two different arguments (i.e., distribution convective "lengths") as in Eq. (9) then allows complete replication of the flame-sheet modeling results for this geometry. By a similar process, this convected disturbance model can be shown to duplicate the flame-sheet results for bluff body V-flames and axisymmetric conical flames as well, differing as discussed previously only in the forms for the characteristic function $V(\lambda)$.

Given the simplicity of this model, some additional discussion of the limiting assumptions is warranted. As stated, this modeling approach encapsulates the results from a linearized flame-sheet model solution. The use of "linearized" in this case is limiting, in that the result of Eq. (14) depends explicitly on the linear relationship between velocity and heat release rate [Eq. (12)]. No attempt to address the nonlinear flame response is attempted here, thus inheriting all the limitations common to linear systems analysis, such as the inability to predict limit cycle behaviors or actual unstable amplitudes. The second significant feature of this approach is the reliance on an external model to produce the heat release rate profile. Therefore, this model does not provide a direct link to flame physics, such as flame surface propagation, that produce the heat release rate profile geometry in flame-sheet modeling. As a result, the local heat release response cannot immediately be tied to be the result of a specific physical behavior described by other models (e.g., local wrinkling of the flame surface). The strength of the convective disturbance approach in light of these limitations is really in the generality of descriptions that it can provide. While the flame heat release rate geometry does not naturally arise from a physical description, it can be more easily tied to experimentally produced profiles that may be more complex than that produced by a simple flame-sheet model. It is hoped that this generality can provide a more complete phenomenological description of the features of experimentally measured flame transfer functions than currently exists, with an eye to steering further model development.

IV. Results and Discussion

Given the knowledge that flame-sheet and convective disturbance modeling approaches produce the same dynamics, it may be useful to offer a brief redescription of the flame-sheet model results within the context of convective disturbances. The characteristic function argument λ corresponds to the position of the downstream edge of the flame in the convective time reference frame. The convective time reference frame depends on both a velocity and length scale [see Eq. (12)]. So, as described previously in literature, the flame-sheet global response to velocity perturbations [Eq. (9)] describes the simultaneous convection of two velocity disturbances through the flame, each of which produce a local disturbance to the surface area proportional both to the surface area per unit axial distance and the amplitude of the velocity disturbance. The flame wrinkle response corresponding to the argument St/β occurs even for a uniform velocity perturbation [evidenced in Eq. (7)]. Recalling the relationship between β and the flame angle, this component of the response is scaled to the convection along the whole flame length using a length calculated along the incline and the decomposed velocity component along the same flame angle. The response with argument KSt occurs only due to the explicit convective velocity forcing and corresponds to convective scaling by the axial length of the flame and the axial flow velocity. Also note that the responses occur in opposite directions (i.e., are separated by 180 deg of phase), with the flame wrinkle response in-phase with the disturbance. Many insights into the nature of the flame transfer functions reported in literature are available from this description.

A. Characteristic Length Scales

Additionally, this model provides some significant insights relative to identification of dominant physical length scales. Consider a convective disturbance model case represented by a simple top-hat distribution subject to a velocity disturbance. Sinusoidal velocity

disturbances are shed an arbitrary distance d upstream of the flame anchoring location and convect at constant velocity u_c.

$$\psi(\tau) = \left[H\left(\tau - \frac{d}{u_c}\right) - H\left(\tau - \frac{L_f + d}{u_c}\right) \right] \tag{16}$$

By investigating the transfer function (i.e., Fourier transform) of this distribution for varying d, we can see that in fact two different, independent length scales are important. One length scale, L_f, is related to the axial length of the heat release region, and the second, x_{com}, is related to the axial distance from the disturbance shedding location to the heat release weighted flame center of mass. To clarify regarding the center of mass, x_{com} is calculated in the same way as a traditional solid body center of mass, excepting use of the local heat release rate intensity as the weighting function in place of density. In the case of the top-hat profile, x_{com} takes a value of d plus one-half the flame length. By observing the flame transfer functions for the different Strouhal numbers using these length scales [inserted in place of x_c in Eq. (2)], the relative importance of these two length scales becomes clearly evident, as shown in Fig. 3. The flame length–based Strouhal number and the center of mass–based Strouhal number are as follows, respectively:

$$St_{Lf} = \frac{\omega L_f}{u_c} \quad \text{and} \quad St_{\text{com}} = \frac{\omega x_{\text{com}}}{u_c}$$

When we use the axial length of the reaction region as characteristic length, as shown on the left in Fig. 3, the slope of the phase varies significantly corresponding to the additional delays associated with the pre-flame convection distance. The magnitude, however, remains unchanged, indicating that the characteristics of the magnitude are unaffected by the downstream shifting of the flame heat release rate profile. Rather, the magnitude behavior is determined only by the spatial interference of the local disturbances in the global heat release rate, an effect that only depends on the relationship between the convective wavelength and the actual length of the reaction region (shape being constant in this case). In contrast, if the flame center of mass from the shedding point is used as the characteristic length as in Fig. 3 on the right, though the magnitude has significant variability in frequency, the slope of the phase at low frequencies is constant. Further analysis shows that this effect occurs independently of the heat release rate distribution's specific shape; all heat release distributions tested exhibited a low-frequency phase slope of −1, corresponding exactly to convection from the shedding location to the effective flame position (i.e., center of mass) at the convection speed u_c.

Thus, for a fixed heat release rate distribution, the modeled dynamics are determined by these two governing length scales. This result is somewhat intuitive. When integrating over the convective field to obtain the global heat release rate (i.e., the magnitude), only regions where the flame exists will have a value, meaning that the actual nature of the magnitude depends only on the flame region itself. However, the timing of those perturbations depends on the complete time history of the disturbances from the moment they originate. Therefore, both Strouhal numbers will be applied in subsequent presentation of flame transfer functions to reflect this behavior; the flame length–based Strouhal number is used for the magnitude, and the center of mass–based Strouhal number is used for the phase.

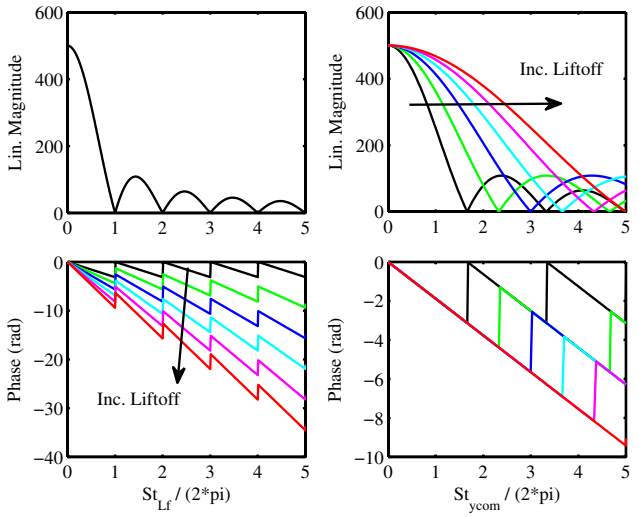

Fig. 3 FTF for different characteristic length: (left) flame length (right) center of mass.

B. Influence of the Heat Release Rate Distribution Shape

Investigation of varied shapes of the heat release rate distributions show the impact of this distribution shape on the predicted flame dynamics. Figure 4 shows several hypothetical heat release profiles, with their global flame transfer functions in Fig. 5. The "experimental fit" profile is loosely based on a curve fit of the mean axial intensity measured from an OH* chemiluminescence flame image. While more advanced analysis of the applicability of convected disturbance models to experimental data is left as an area for future study, this is provided here as an example of the response for a heat release profile akin to that seen in a basic experimental configuration. Analytical expressions for these transfer functions are easily obtainable from their definitions and are summarized in Table 1.

When using the flame length as the characteristic length, for each of these fixed geometries the flame transfer functions are observed to depend only on the convective length of the reaction region St_{Lf}. Further, similarities in the magnitude exist in that all transfer functions maintain the overall low-pass filter characteristic due to the diminishing convective wavelength of the disturbances as excitation frequency increases. However, the frequencies at which a zero crossing occurs in magnitude (if one occurs at all) vary between a Strouhal number of 1.0 and 2.0 depending on the geometry. Two of these cases (linear and experimental approximation) have no zero crossings at all, due to the asymmetry of those profiles, preventing complete spatial interference from occurring. This observation indicates that the actual distribution of heat release rate has a significant influence on the dynamic response that cannot be completely captured by a single characteristic length.

The phase of these transfer functions is shown relative to the center of mass scaling. While Strouhal numbers of the phase dynamics do not directly correlate to those in the magnitude because of this scaling, we can notice that all profiles have the same low frequency phase slope of negative unity. This reinforces that even for different

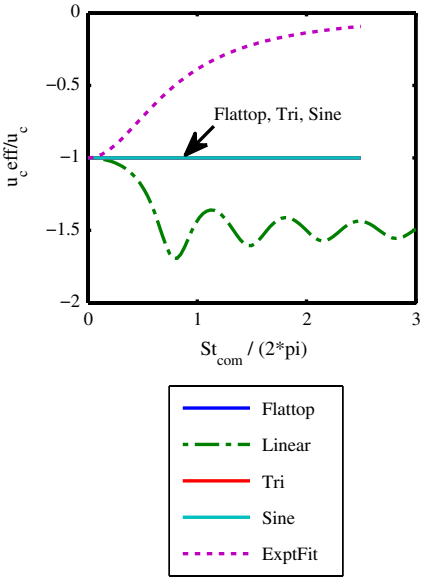

Fig. 4 Variation in calculated convective velocity with respect to Strouhal number.

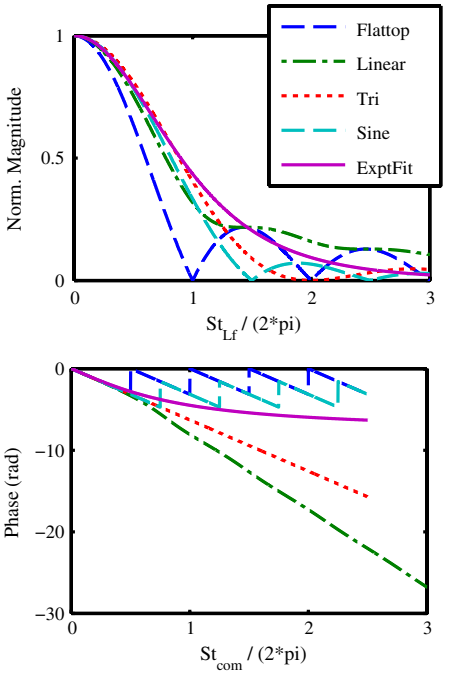

Fig. 5 Sample FTFs $V(\lambda)$ for profiles in Fig. 4.

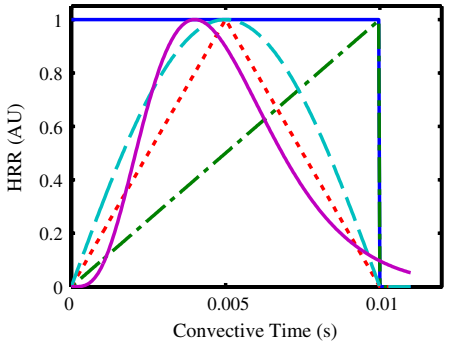

Fig. 6 Sample heat release profiles. Experimental approximation uses $a = 4$ and $b = 333$.

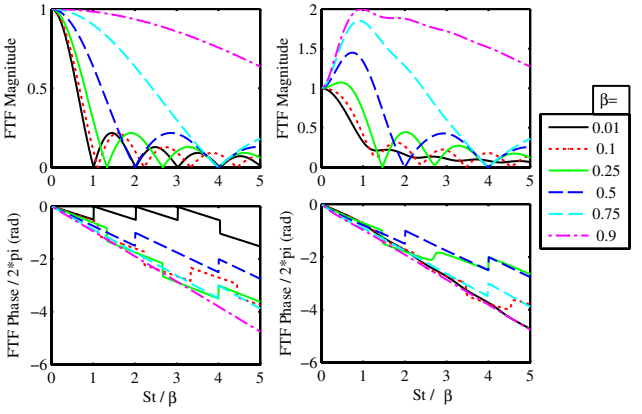

Fig. 7 FTF shape with varying β. (left) Bluff body V-flame (right) axisymmetric V-flame.

profile shapes the timing of the flame response is delayed by the disturbance reaching the center of mass, which serves as an effective flame position. Note that the center of mass for an asymmetric profile is **not** equivalent to the position of maximum heat release rate, but instead represents the actual average position of the heat release rate. With increasing frequency, dynamic characteristics may begin to affect the phase slope, as shown in Fig. 6, which makes identification of convective velocity from the group delay difficult.

C. Nonconstant Velocity

It is possible to consider velocity distributions $u_c(x)$, which are not constant. By inspection of Eq. (11), we can observe that this essentially produces a nonuniform convective time coordinate, which impacts the calculation of the heat release rate profile in convective time. Transformation of the spatial heat release rate profile into one based on convective time then requires inversion of $\tau(x)$ and substitution as in the following expression:

$$\psi(\tau) = \psi(x(\tau)) \tag{17}$$

This produces a profile $\psi(\tau)$ that is locally stretched relative to its spatial form, in accordance with variations in the local convective velocity. While this impacts the dynamics due to changes in the shape of the flame profile, as discussed in the preceding section, no unique dynamic behaviors are introduced.

D. Multiple Perturbations

We can also consider the effects of multiple perturbations on the transfer function response, especially as guided by the results from flame-sheet modeling [Eq. (9)]. Due to the linear nature of the effects considered in this model, the occurrence of multiple perturbations results in superposition of the individual responses. Further, since the Fourier transform is in itself a linear operation, superimposed responses can be characterized by considering superimposed flame heat release rate profiles. When multiple perturbations occur, we can calculate an effective profile representing these combined effects. A more detailed description of this process can be found in the Appendix.

One interesting feature described in literature for the cases resulting in multiple disturbance responses like that in Eq. (9), is the possibility of resonance-like gain in the magnitude of the transfer function. Consider, for example, the results in Fig. 7, which show the flame transfer function for multiple perturbations described in Eq. (9) for both bluff body V-flames and axisymmetric V-flames (flat-top profile and linear profile, respectively), similarly to Preetham et al. [21]. In the case of axisymmetric flames, amplified gain appears for values of β greater than about 0.25. Interestingly, bluff-body stabilized flames do not exhibit this amplified gain for any conditions.

To further investigate the origin of this amplification, we consider the heat release rate profiles described by the response in Eq. (9): a flame wrinkle convected along the flame surface and a bulk flow convective perturbation. These profiles for each case are shown in Fig. 8. The most notable aspect of these profiles is that the bluff body stabilized flame, which does not exhibit resonant behavior, exhibits

Table 1 Summary of flame transfer functions and profiles for the profiles shown in Fig. 4

Profile	Normalized HRR profile—$\psi(\tau)$	$F(\lambda)/\bar{Q}$
Flat	$H(t-0) - H(t-\lambda/\omega)$	$\frac{1}{j\lambda}[1 - e^{-j\lambda}]$
Linear	$\frac{t\omega}{\lambda}[H(t-0) - H(t-\lambda/\omega)]$	$\frac{-2}{\lambda^2}[1 - e^{-j\lambda}(1 + j\lambda)]$
Triangular	$2\frac{t\omega}{\lambda}[H(t-0) - H(t-\lambda/2\omega)] + (2 - 2\frac{t\omega}{\lambda})[H(t-\lambda/2\omega) - H(t-\lambda/\omega)]$	$-\frac{4}{\lambda^2}[1 - e^{-j\frac{\lambda}{2}}]^2$
Half sine	$\sin(\frac{\pi\omega}{\lambda}t)[H(t-0) - H(t-\lambda/\omega)]$	$\frac{\pi^2}{2\pi^2 - 2\lambda^2}(1 + e^{-j\lambda})$
Expt. fit	$t^a e^{-bt}$	$(\frac{b}{b+j\lambda})^{a+1}$

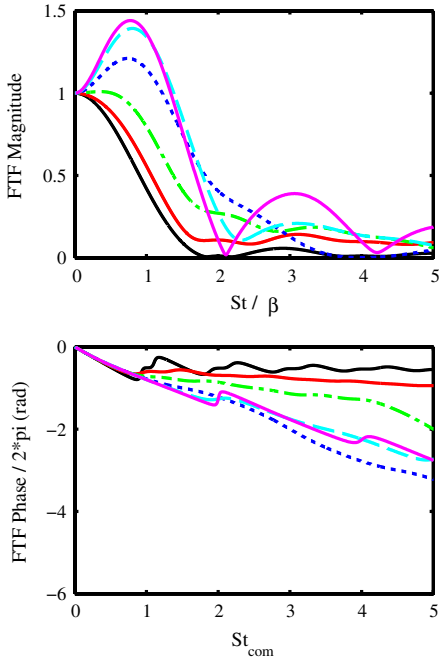

Fig. 8 Nondimensionalization of triangular profile FTFs using St/β as characteristic length.

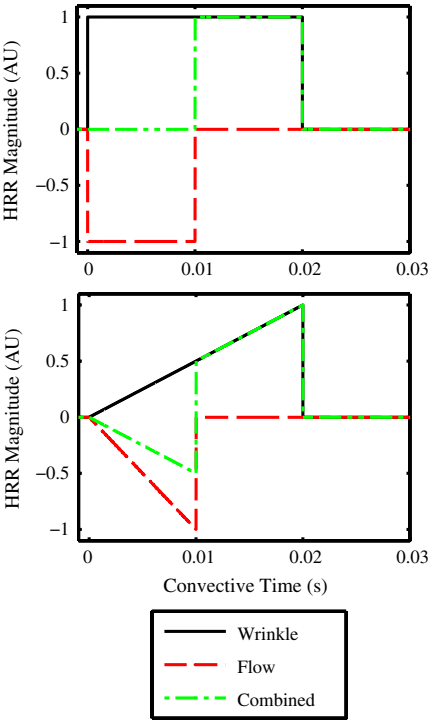

Fig. 9 Sample effective heat release rate profiles for $K = 1$, $\beta = 0.5$.

only a net positive profile region. In contrast, the axisymmetric flame has both positive and negative portions. By testing various profiles and combinations, it can be observed that this is a necessary feature for amplifying gain to occur. Further, inspection of Fig. 7 reveals that for convection at the flow velocity, as β approaches unity (the two disturbances travel at the same speed), the bandwidth of the response approaches infinity.

This effect can also be explained considering the results in Fig. 8. For β approaching unity, the curves representing the wrinkle and the flow become more and more similar. This means that the combined profile becomes more and more similar to an impulse, for which the effective flame length is zero. As an impulse has a Fourier transform of unity, it is unsurprising then to see bandwidths approach infinity. The phase, however, approaches a limit value corresponding to convection of the disturbance to the tail edge of the flame where the effective impulse is located. We can apply nondimensionalizations by an effective flame length and the center of mass for the combined profiles to create the transfer function plots in Fig. 9. As evident, the bluff-body V-flame possesses a single magnitude response irrespective of the value of β, as could be expected based on the shape of the net profile in Fig. 8. The axisymmetric flame has a reasonable frequency collapse over the range of β considered, though exhibits variability due to the influence of the changing negative valued region. In both cases, the low frequency phase slope is, as expected, scaled perfectly with the previously discussed value of -1. Dynamic effects begin to influence the phase around a St_{com} value of approximately 0.5, providing some insight into the limits on what range of Strouhal numbers provide suitable indications of the group delay.

Some further discussion is warranted on the concept of effective lengths for these combined profiles. Calculating center of mass for a profile including even a negative heat release region is straightforward, if somewhat physically nonintuitive. The low-frequency slope of the transfer function phase is therefore obtainable using established techniques, even for an arbitrary profile. Effective flame length, however, does not possess an easily discernable universal definition. In the case of the bluff body V-flame (Fig. 8, top), the combined flame length is observed as the difference in convective flame lengths between the two constituent profiles. In the absence of a clear correspondence in the case of the axisymmetric V-flame, the same length as in the bluff-body case was used to reflect the similarity in the impulse-like shape of the combined response, resulting in the reasonably successful scaling seen in Fig. 9. However, investigation shows that this same characterization is unsuccessful for profiles that tend toward zero at the tail end of the flame. Consider, for example, the case of the symmetric triangular profile. While normalization by the distance between the tail ends of the two component profiles is unsuccessful, normalization by the length of the longer profile is reasonably effective. This result is shown in Fig. 10.

Further investigation and generalization is still needed to determine whether there is some general scaling law of which these two observations are a subset. At present, however, the described trends appear to hold true for the set of profiles investigated here. Transfer function magnitudes for profiles that have a sharp tail edge can be normalized using the distance between the profile tail edges, taking a value of $L_{\text{eff}} = L(1/\beta - K)$. Profiles with zero intensity at the tail edge of the flame have transfer function magnitudes that best are normalized using the convective length of the flame wrinkle profile $L_{\text{eff}} = L(1/\beta)$.

E. Ramifications and Future Usefulness

The greatest significance of this work lies in the physical ramifications it implies for known results from linearized flame-sheet

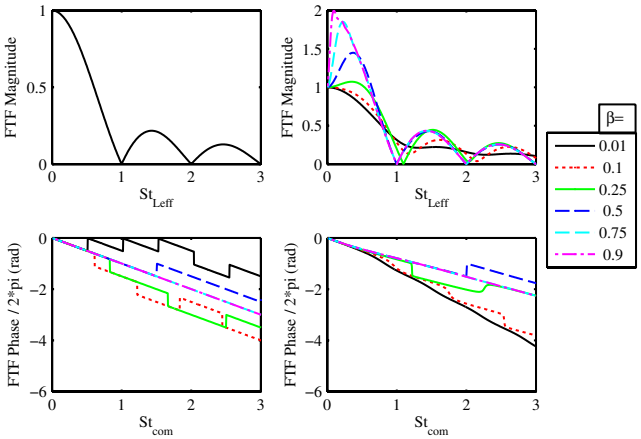

Fig. 10 Improved nondimensionalization for two geometries (left) bluff body V-flame (right) axisymmetric V-flame.

modeling. Though flame-sheet model solutions represent the dynamics of a time-dependent differential equation, the heat release rate behaviors described can actually be inferred from the *steady* heat release rate profile, as described by the pertinent flame geometry. The transfer function physics modeled by flame-sheet approaches are identical to those shown by a convected disturbance model, highlighting the influence of convective phenomena and the need to pay careful attention to the actual geometry of the flame being modeled in comparisons of results.

The importance of the steady heat release rate profile has significant potential for use of experimental measurements or computational fluid dynamics (CFD) flame simulations. While the oscillating flame position may be measured by established techniques, it is a much simpler proposition to obtain a single, time-averaged snapshot of the flame heat release rate intensity. Likewise, acoustically oscillating numerical modeling of flames is computationally taxing and may be prohibitive depending on the frequencies considered. Future validation of convective disturbance models may provide an avenue by which time-averaged diagnostics and computational techniques can still result in the necessary dynamic understanding for making thermoacoustic instability predictions.

Further, in terms of guidance to experimental flame transfer function interpretation, the insight provided by the convective disturbance model has the potential to aid in analysis and identification of the underlying physics represented by measured flame transfer functions. For example, by performing an inverse Fourier transform on a known flame transfer function, one may predict the theoretical heat release rate profile that would produce the measured dynamics. By assuming a set number of perturbations, their effective origins and convective speeds could then in principle be calculated from this effective heat release profile by a set of linear combinations of a measured static flame heat release rate profile. This type of analysis could be extremely helpful in identifying general flame dynamic behaviors that could be compared across experimental conditions and geometries.

V. Conclusions

The convected disturbance modeling approach allows analysis of flame response to disturbances with a more general set of parameters (or more accurately, heat release rate geometries) than currently reported for flame-sheet model efforts. This includes the potential for direct computation of flame dynamics from static heat release profiles, which could ultimately be obtained either from experiments or numerical flame models. Scrutiny of preliminary convected disturbance model results revealed several underlying behaviors that can guide further analysis of flame dynamics.

The basic dynamic characteristics of the flame transfer function magnitude are determined by the convective/spatial nature of the velocity perturbations. The length scale characterizing the magnitude therefore relates to the leading-edge to tail-edge length of the heat release profile. This fact is especially significant in lifted geometries in which the presence of a liftoff distance would not be expected to affect the characteristics of the transfer function magnitude. Multiple perturbations create a complicated situation in which it becomes much more difficult to identify a generalized effective characteristic length. For these cases, a two-part approach was used for nondimensionalization. Profiles having a sharp tail-edge shape were nondimensionalized using the difference between the convective lengths associated with the two perturbations considered. Profiles with a tail-edge value trending toward zero were scaled by the total length of the profile. Generalization of these effects is a potential area for continued study of convected disturbance model efforts.

The phase dynamics were found to be scalable in a more general way. The low frequency slope of the phase corresponded exactly to convection at the mean convective velocity from the disturbance origin to the center of mass of the flame heat release region. In this regard, the flame center of mass can be considered as the mean location of the flame. Relative to lifted flame geometries, this implies that the liftoff distance does introduce additional delay. The scalability of phase by flame center of mass held even when considering situations with multiple disturbances. These insights on the phase slope are limited to what occurs at low frequency, before dynamic effects alter the behavior. However, they do provide a simple, general behavior that can be analyzed regardless of the nature of the disturbances or the flame-sheet. As such, the low frequency phase behavior provides an apparently "friendly" starting point for comparison between models and experimental data.

Due to the simplicity of predicting dynamics directly from steady heat release rate profiles, determination of flame transfer functions based on this modeling approach may be a suitable candidate for active sensor and control applications. However, in order to achieve this, extended experimental validation of these results (likewise with flame-sheet model results) is extremely important. Continued study of convected disturbance models is necessary, especially with regard to investigation of application of this modeling approach to identification of flame dynamics in experiments.

Appendix: Combination of Multiple Profiles

Note that combining two profiles into an effective profile is not as simple as adding together two profiles with the coefficients in Eq. (9). Recall that each characteristic function is the Fourier transform of a profile normalized by its mean heat release. When finding the combination of two profiles that leads to the transfer function, we are really looking for an effective third profile as follows:

$$\begin{aligned}\mathrm{FTF} &= \frac{1}{A+B}[AF(\lambda_1) + BF(\lambda_2)] \\ &= \frac{1}{A+B}\left[A\frac{\Psi(\lambda_1)}{\int \psi(\lambda_1)\,\mathrm{d}\lambda} + B\frac{\Psi(\lambda_2)}{\int \psi(\lambda_2)\,\mathrm{d}\lambda}\right] = \frac{\Psi(\lambda_3)}{\int \psi(\lambda_3)\,\mathrm{d}\lambda}\end{aligned}$$

Neglecting the absolute scaling on the new function and taking the inverse Fourier transform, we then find

$$\psi(\lambda_3) \propto A\psi(\lambda_1)\int \psi(\lambda_2)\,\mathrm{d}\lambda + B\psi(\lambda_2)\int \psi(\lambda_1)\,\mathrm{d}\lambda$$

So for the cases of the flame-sheet approximations, the desired combined profile appears as follows:

$$\psi(\lambda_3) \propto K\beta\psi(KSt)\int \psi\left(\frac{St}{\beta}\right)\mathrm{d}St - \psi\left(\frac{St}{\beta}\right)\int \psi(KSt)\,\mathrm{d}St$$

The notable feature here is that the integral heat release rates of the individual profiles are required to correctly scale the effective response. In the case of the flame-sheet combinations, this somewhat surreptitiously results in equivalence between the absolute value of the peak intensity values of each profile.

Acknowledgments

The support of the U.S. Department of Energy's Turbines program is gratefully acknowledged. Joseph A. Ranalli gratefully acknowledges the support of the Oak Ridge Institute for Science and Education (ORISE) Postdoctoral Fellowship program.

References

[1] Lieuwen, T. C., and Yang, V., *Combustion Instabilities in Gas Turbine Engines: Operational Experience, Fundamental Mechanisms, and Modeling*, AIAA, Reston, VA, 2005, pp. 147–162.

[2] Lieuwen, T., "Modeling Premixed Combustion–Acoustic Wave Interactions: A Review," *Journal of Propulsion and Power*, Vol. 19, No. 5, 2003, pp. 765–781. doi:10.2514/2.6193

[3] Ducruix, S., Durox, D., and Candel, S., "Theoretical and Experimental Determinations of the Transfer Function of a Laminar Premixed Flame," *Proceedings of the Combustion Institute*, Vol. 28, No. 1, 2000, pp. 765–773. doi:10.1016/S0082-0784(00)80279-9

[4] Palies, P., Durox, D., Schuller, T., and Candel, S., "The Combined Dynamics of Swirler and Turbulent Premixed Swirling Flames," *Combustion and Flame*, Vol. 157, No. 9, 2010, pp. 1698–1717. doi:10.1016/j.combustflame.2010.02.011

[5] Lohrmann, M., and Buchner, H., "Prediction of Stability Limits for LP and LPP Gas Turbine Combustors," *Combustion Science and Technology*, Vol. 177, No. 12, 2005, pp. 2243–2273. doi:10.1080/00102200500241040

[6] Kim, D., and Park, S. W., "Effects of Hydrogen Addition on Flame Structure and Forced Flame Response to Velocity Modulation in a Turbulent Lean Premixed Combustor," *Fuel*, Vol. 89, No. 11, 2010, pp. 3475–3481. doi:10.1016/j.fuel.2010.06.021

[7] Ranalli, J., Martin, C., Black, P., Vandsburger, U., and West, R., "Measurement of Flame Transfer Functions in SwirlStabilized, Lean-Premixed Combustion," *Journal of Propulsion and Power*, Vol. 25, No. 6, 2009, pp. 1350–1354. doi:10.2514/1.44187

[8] Ranalli, J., and Ferguson, D., "Measurement of Flame Frequency Response Functions in a Low-Swirl Flame under Exhaust Gas Recirculation Conditions," AIAA Paper 2011-518, 2011.

[9] Durox, D., Schuller, T., and Candel, S., "Combustion Dynamics of Inverted Conical Flames," *Proceedings of the Combustion Institute*, Vol. 30, No. 2, 2005, pp. 1717–1724. doi:10.1016/j.proci.2004.08.067

[10] Balachandran, R., Ayoola, B. O., Kaminski, C. F., Dowling, A. P., and Mastorakos, E., "Experimental Investigation of the Nonlinear Response of Turbulent Premixed Flames to Imposed Inlet Velocity Oscillations," *Combustion and Flame*, Vol. 143, Nos. 1–2, 2005, pp. 37–55. doi:10.1016/j.combustflame.2005.04.009

[11] Kim, K. T., Lee, J. G., Quay, B. D., and Santavicca, D. A., "Spatially Distributed Flame Transfer Functions for Predicting Combustion Dynamics in Lean Premixed Gas Turbine Combustors," *Combustion and Flame*, Vol. 157, No. 9, 2010, pp. 1718–1730. doi:10.1016/j.combustflame.2010.04.016

[12] Külsheimer, C., and Büchner, H., "Combustion Dynamics of Turbulent Swirling Flames," *Combustion and Flame*, Vol. 131, Nos. 1–2, 2002, pp. 70–84. doi:10.1016/S0010-2180(02)00394-2

[13] Shanbhogue, S., Shin, D., Hemchandra, S., Plaks, D., and Lieuwen, T., "Flame–Sheet Dynamics of Bluff–Body Stabilized Flames During Longitudinal Acoustic Forcing," *Proceedings of the Combustion Institute*, Vol. 32, No. 2, 2009, pp. 1787–1794. doi:10.1016/j.proci.2008.06.034

[14] Dowling, A. P., "A Kinematic Model of a Ducted Flame," *Journal of Fluid Mechanics*, Vol. 394, Sept. 1999, pp. 51–72. doi:10.1017/S0022112099005686

[15] Baillot, F., Durox, D., and Prud'homme, R., "Experimental and Theoretical Study of a Premixed Vibrating Flame," *Combustion and Flame*, Vol. 88, No. 2, Feb. 1992, pp. 149–168. doi:10.1016/0010-2180(92)90049-U

[16] Boyer, L., and Quinard, J., "On the Dynamics of Anchored Flames," *Combustion and Flame*, Vol. 82, No. 1, 1990, pp. 51–65. doi:10.1016/0010-2180(90)90077-5

[17] Fleifil, M., Annaswamy, A. M., Ghoneim, Z. A., and Ghoniem, A. F., "Response of a Laminar Premixed Flame to Flow Oscillations: A Kinematic Model and Thermoacoustic Instability Results," *Combustion and Flame*, Vol. 106, No. 4, 1996, pp. 487–510. doi:10.1016/0010-2180(96)00049-1

[18] You, D., Huang, Y., and Yang, V., "A Generalized Model of Acoustic Response of Turbulent Premixed Flame and Its Application to Gas–Turbine Combustion Instability Analysis," *Combustion Science and Technology*, Vol. 177, No. 5–6, 2005, pp. 1109–1150. doi:10.1080/00102200590927012

[19] Palies, P., Schuller, T., Durox, D., and Candel, S., "Modeling of Premixed Swirling Flames Transfer Functions," *Proceedings of the Combustion Institute*, Vol. 33, No. 2, 2011, pp. 2967–2974. doi:10.1016/j.proci.2010.06.059

[20] Schuller, T., Durox, D., and Candel, S., "A Unified Model for the Prediction of Laminar Flame Transfer Functions: Comparisons Between Conical and V-Flame Dynamics," *Combustion and Flame*, Vol. 134, Nos. 1–2, 2003, pp. 21–34. doi:10.1016/S0010-2180(03)00042-7

[21] Preetham, H. S., and Lieuwen, T., "Dynamics of Laminar Premixed Flames Forced by Harmonic Velocity Disturbances," *Journal of Propulsion and Power*, Vol. 24, No. 6, 2008, pp. 1390–1402. doi:10.2514/1.35432

[22] Jones, B., Lee, J. G., Quay, B. D., and Santavicca, D. A., "Flame Response Mechanisms Due to Velocity Perturbations in a Lean Premixed Gas Turbine Combustor," *Journal of Engineering for Gas Turbines and Power*, Vol. 133, No. 2, 2011, pp. 323–333. doi:10.1115/GT2010-22380

[23] Kim, K. T., Lee, J. G., Lee, H. J., Quay, B. D., and Santavicca, D. A., "Characterization of Forced Flame Response of Swirl–Stabilized Turbulent Lean-Premixed Flames in a Gas Turbine Combustor," *Journal of Engineering for Gas Turbines and Power*, Vol. 132, No. 4, 2010, pp. 041502–041508. doi:10.1115/1.3204532

[24] Johnson, M. R., Littlejohn, D., Nazeer, W. A., Smith, K. O., and Cheng, R. K., "A Comparison of the Flowfields and Emissions of High-Swirl Injectors and Low-Swirl Injectors for Lean Premixed Gas Turbines," *Proceedings of the Combustion Institute*, Vol. 30, No. 2, 2005, pp. 2867–2874. doi:10.1016/j.proci.2004.07.040

[25] Cheng, R. K., Littlejohn, D., Strakey, P. A., and Sidwell, T., "Laboratory Investigations of a Low-Swirl Injector with H2 and CH4 at Gas Turbine Conditions," *Proceedings of the Combustion Institute*, Vol. 32, No. 2, 2009, pp. 3001–3009. doi:10.1016/j.proci.2008.06.141

A. Gupta
Associate Editor